CrystEngComm

Accepted Manuscript

ROYAL SOCIETY OF CHEMISTRY

www.rsc.org/crystengcomm

ARTICLE TYPE www. rsc.org/xxxxxx | XXXXXXXX

Polar and antiferroelectric behaviour of a hybrid crystal – Piperazinium perchlorate

Maciej Wojtaś,*[a] Anna Gągor,[b] Olaf Czupiński,[a] Anna Piecha-Bisiorek,[a] Dmitry Isakov,[c] Wojciech Medycki,[d] and Ryszard Jakubas[a]

Received Xth XXXXXXXXXX 20XX, Accepted Xth XXXXXXXXX 20XX
First published on the web Xth XXXXXXXXXX 200X
DOI: 10.1039/b000000x

Monoprotonated piperazinium perchlorate, $[NH_2(CH_2)_4NH][ClO_4]$, appeared to be a novel room temperature polar material ($P1$). Its acentric symmetry was confirmed by a single crystal X–ray diffraction, second harmonic generation (SHG) and pyroelectric measurements. Differential scanning calorimetry (DSC) measurements revealed complex sequence of phase transitions above room temperature: I↔II at 433/422 K (heating-cooling), II↔III – 417/411 K, III↔IV – 403/395 and IV↔V at 397 (the lowest temperature phase transition recorded only upon heating). The characteristic feature of the structure of $[NH_2(CH_2)_4NH][ClO_4]$ is the presence of two parallel cationic chains which are connected with each other by strong N—H…N hydrogen bonds. In phase V these strongly polar non–equivalent chains contribute to the spontaneous polarization. ^{1}H NMR measurements disclosed the reorientational motions of the piperazinium ($[NH_2(CH_3)NH]^+$) cations as well as the proton motion in the N—H…N hydrogen bonds along the piperazine chain. Over the phase I the overall motions of the ClO_4^- anions, and reorientational motion of cations are postulated. The dielectric response, ε'(T), accompanying the PT I↔II indicates possible antiferroelectricity in the phase II.

1 Introduction

Materials that may be characterized by extraordinary electrical properties are of great interest because of their importance in novel technologies. For instance, just to name a few, high values of dielectric permittivity exhibited by some of these electrically ordered materials make them important in development of dielectric resonators and filters for microwave communication systems[1]. One of the most interesting group of such materials, from this point of view, are ferroelectrics i.e. compounds where in some temperature range one may observe reversible spontaneous polarization[2]. This effect is due to certain arrangement of molecules, ions etc. in crystal structure and may be observed only in polar phases. High values of dielectric permittivity are often observed in other crystals—antiferroelectrics. Antiferroelectrics are apolar materials which crystal structure exhibit inversion center but the strong external electric field can deform internal structure and induce ferroelectricity[3].

Taking into account the potential application of such materials at issue is to maintain the stability of electrically ordered phases near or above room temperature. In the group of the most promising substances possessing these desired properties are hybrid inorganic–organic materials. The combination of the inorganic frameworks (electronic properties) and the intriguing features of the organic molecules (flexibility and the ability to form weak interactions) may lead to obtain compounds which the Curie temperature, T_C, is above room temperature[4–6].

As a matter of fact many simple ionic inorganic–organic (1:1) hybrid complexes were found to exhibit interesting ferroelectric properties at room temperature. They contain in crystal structure various heterocyclic aromatic cations (pyridinium, imidazolium)[7–11] or non-aromatic (e.g. dabco 1,4-diaza-bicyclo[2.2.2]octane) cations[12–14] and tetrahedral anions: BF_4^-, ClO_4^-, ReO_4^-, IO_4^- and CrO_3F^-. However, it seems worthy of note that there are known just few inorganic–organic hybrid crystals which are anitiferroelectric ones. Currently the most numerous group of organic antiferroelectrics are liquid crystals, see for example the article of I. Nishiyama[15] and references therein.

In this paper we present results of investigations carried out for new piperazinium compound synthesized: piperazin-1-ium perchlorate ($[Pip][ClO_4]$). This crystal is an example of rarely encountered compounds of single protonated piperazine with simple inorganic acid. The DSC studies showed that the title crystal exhibits a rich polymorphism in the solid state.

[a] *Faculty of Chemistry, University of Wrocław, 14 Joliot–Curie, 50–383 Wrocław, Poland; E-mail: maciej.wojtas@chem.uni.wroc.pl*
[b] *W. Trzebiatowski Institute of Low Temperature and Structure Research Polish Academy of Science, PO Box 1410, 50-950 Wrocław, Poland.*
[c] *Universidade do Minho, Centro de Fisica, Campus de Gualtar, 4710-057 Braga, Portugal*
[d] *Institute of Molecular Physics, Polish Academy of Science, Smoluchowskiego 17, 60-179 Poznań, Poland*

The crystal structure was determined by means of the X–ray diffraction measurements, SHG and pyroelectric measurements proved the polar character of room temperature phase, in turn the dielectric spectroscopy results strongly suggest the existence of antiferroelectricity in one of the intermediate phase. The molecular mechanism of phase transitions (PTs) was analyzed by ^{1}H NMR studies.

2 Experimental

The piperazine hexahydrate, $[NH(CH_2)_4NH]\cdot 6H_2O$ (Fluka) was solubilized in concentrated $HClO_4$ (70%, AppliChem). The compound was recrystallized twice from the solution and the single crystals were grown at constant room temperature by slow evaporation. Elemental analysis was performed by means of the commercial CHNS vario EL III Elementar apparatus on C, H and N. It was (% exp./theor.): C(25.70/25.74), H(6.01/5.90), N(14.96/15.01). Monocrystals had a shape of a rectangular prism. While working on perchlorate salts the caution is counseled due to their health hazard and potential explosiveness.

Differential Scanning Calorimetry (DSC) measurements on powdered samples were carried out using a Perkin–Elmer DSC 8500 in the temperature range 100–470 K with a scan rate of 20 K·min^{-1}. Since the calorimetric measurements did not prove any thermal anomaly below room temperature the subsequent measurements were carried out in the temperature range 300–470 K with the scan rates 20, 10 and 5 deg/min.

TGA and DTA were made on a Setaram SETSYS 16/18 instrument in a nitrogen atmosphere. The sample mass was 12.400 mg, the heating rate 2 K·min^{-1}, and the temperature range 300–700 K.

The complex electric permittivity, $\varepsilon* = \varepsilon' - i\varepsilon''$, was measured by a E4980A Precision LCR Meter within the frequency range 500 Hz–2 MHz and in the temperature range within 300–450 K. The dimensions of the sample were of the order of $5\times3\times1$ mm^3. The overall error for the real and imaginary parts of the complex electric permittivity was less than 5% and 10%, respectively.

The spontaneous polarization was measured by a charge integration technique using a Keithley 617 Programmable Electrometer. The temperature was stabilized by an Instec STC200 temperature controller. The same experimental setup was used in the case of the DC conductivity measurements.

The relative Second Harmonic Generation (SHG) efficiencies of a range of powder particle sizes were measured using the Kurtz and Perry powder technique [16]. In powder test a pulsed Q-switched Nd:YAG laser was utilized to generate fundamental 1064 nm light with pulse energy 22 mJ, width and repetition rate of 20 ns and 10 Hz respectively.

The NMR measurements were made using an ELLAB TEL–Atomic PS 15 spectrometer. Proton spin–lattice relaxation times T_1 at 25 MHz were measured using an appropriate saturation sequence of $\pi/2$ pulses followed by a variable time interval τ and a reading $\pi/2$ pulse. The magnetization was found to recover exponentially within experimental error in whole studied temperature range. The temperature was stabilized by a temperature controller type 660 UNIPAN ($\pm$1 K). The sample of powdered $[Pip][ClO_4]$ was evacuated at room temperature and then sealed under vacuum in a glass ampoule. All measurements were made on heating from liquid nitrogen temperature. The errors in the measurements of T_1 were estimated to be about 5%.

The X-ray diffraction has been done using four–circle KM4CCD diffractometr operating in κ geometry. The details of the crystal data and data collection are presented in table 1. Low temperatures were maintained by the nitrogen gas open–flow system (Oxford Diffraction) whereas the simple hot air flow attachment was applied for high temperatures. The crystals were measured in quartz capillaries in order to protect them against sublimation which could be intensified by the air flow. The CrysAlis CCD and CrysAlis RED [17] were used for data collection and reduction. The absorption correction was done using spherical harmonics, implemented in SCALE3 ABSPACK scaling algorithm. Shelxs97 and Shelxl97 [18] programs were utilized for the solution and refinement of the crystal structure, respectively. The absolute structure parameter y was calculated using PLATON [19].

Due to the presence of disorder of ClO_4^- groups that reflected in statistically occupied multiplied oxygen positions the Cl–O distance restraints were applied during the refinement of the structure. The disorder of the ClO_4^- had also pronounced influence on the reliability R factors which were on the increase with temperature activation of rotations of those groups. All hydrogen atoms were placed in geometrically calculated positions and were not refined due to the pronounced disorder of the anions. Crystallographic data for the structures reported in this paper have been deposited with the Cambridge Crystallographic Data Centre, CCDC no. 1019423 (200 K), 1019424 (413 K) and 1019425 (426 K). Copies of this information may be obtained free of charge from the CCDC, 12 Union Road, Cambridge CB2 1EZ, UK (fax: +44-1223-336033; e-mail: deposit@ccdc.cam.ac.uk or http://www.ccdc.cam.ac.uk).

3 Thermal behavior

DSC traces on cooling and heating are presented in Figure 1a. The sequence of PTs on heating is characterized by four peaks whereas on cooling just by three. This discrepancy is, however, easy to explain. Two lowest temperature peaks on heating related to the PTs V→IV at 397 K and IV→III at 403 K merge into one peak on cooling. This one thermal anomaly on cooling run is due to two PTs what is proofed by the calculated entropy (see Tab. 2) and the fact that all the phase sequence

Table 1 Crystal data, data collection and refinement results for [Pip][ClO_4]

	Phase V	Phase III	Phase II
Crystal Data			
Chemical formula		$[NH_2(CH_2)_4NH][ClO_4]$	
Mr		186.6	
Crystal system, space group	Triclinic, $P1$	Triclinic, $P\bar{1}$	Monoclinic, $C2/m$
Temperature (K)	200	413	426
a, b, c (Å)	7.8955 (8), 7.9685 (10), 12.611 (2)	8.0326 (8), 8.0754 (10), 12.745 (2)	13.047 (8), 9.700 (3), 8.348 (5)
α, β, γ (°)	84.587 (14), 88.678 (14), 76.076 (10)	84.190 (14), 88.360 (14), 76.009 (10)	129.31 (9)
V (Å^3)	766.66 (18)	798.07 (18)	817.5 (7)
Z	4	4	4
Radiation type		Mo Kα	
μ (mm^{-1})	0.47	0.45	0.44
Crystal size (mm)		$0.21 \times 0.19 \times 0.15$	
Data Collection			
No. of measured, independent and observed [I> 2σ(I)] ref.	7672, 4414, 2831	7153, 2987, 1468	4145, 819, 491
Rint	0.016	0.032	0.029
$(\sin\theta/\lambda)_{max}$ (Å^{-1})	0.61	0.61	0.609
Data Refinement			
R[$F^2 > 2\sigma(F^2)$], wR(F^2), S	0.033, 0.104, 0.95	0.049, 0.151, 0.90	0.073, 0.216, 0.96
No. of reflections	4414	2987	819
No. of parameters	398	236	79
No. of restraints	35	11	5
$\Delta\rho_{max}$, $\Delta\rho_{min}$ (e·Å^{-3})	0.41, -0.38	0.36, -0.37	0.43, -0.35
Absolute structure	Classical Flack method preferred over Parsons because s.u. lower.		
Absolute structure parameter	0.22(8) (Flack x parameter)[20] 0.54(9) (Hooft y parameter)[21]		

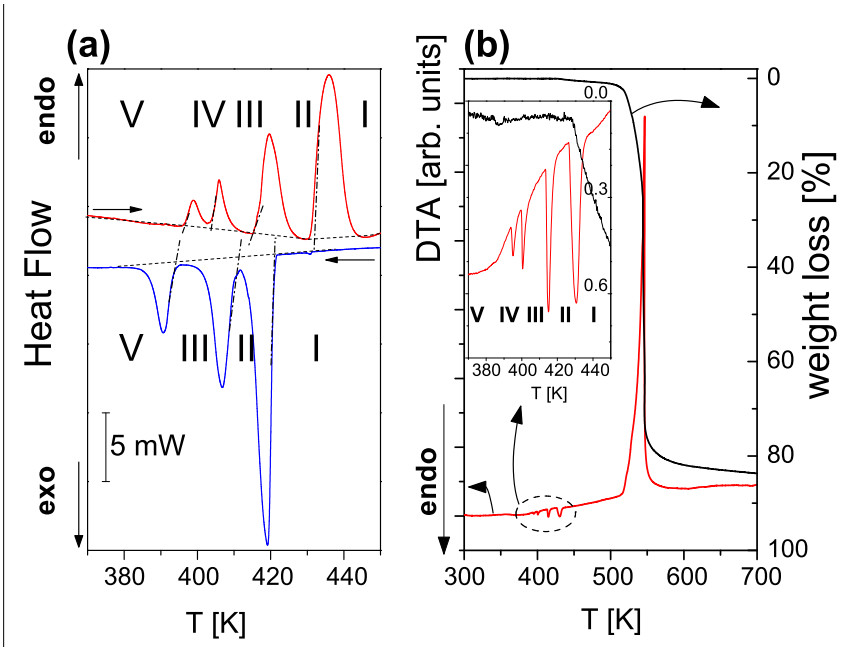

Fig. 1 (a) DSC curves of $[Pip][ClO_4]$ on heating and cooling runs and (b) simultaneous curves of thermogravimetric analysis and differential thermal analysis (3 K·min^{-1}). Note that the endoenergetic peaks in DSC and TGA are presented reversely.

Table 2 Parameters of PTs of $[Pip][ClO_4]$ recorded on heating and cooling runs with the rate 5 deg/min. Note that the values of Temp. and ΔS of the lowest temperature PT on cooling (V←IV&IV←III PTs) are given in the third row from the bottom of the table.

	Heating		Cooling	
Phase transition	Temp. [K]	ΔS [J·mol^{-1}·K^{-1}]	Temp. [K]	ΔS [J·mol^{-1}·K^{-1}]
V↔IV	397	1.4	*V←IV & IV←III PTs*	
IV↔III	403	2.2	395	3.5
III↔II	417	7.1	411	7.4
II↔I	433	14.4	422	14.6

from phase V to I is fully reproducible and reversible. In the table below (Tab. 2) the phase transition parameters are presented. In order to examine the thermal stability of $[Pip][ClO_4]$ the thermogravimetry method was applied. The simultaneous curves of differential thermal analysis (DTA) and mass of the sample vs. temperature is presented in figure 1b. One may see four thermal anomalies observed already by means of DSC method. It is worth noting that the decomposition process starts at II→I PT temperature. However, at this temperature this process is still very slow and the weight loss amounts to ca 0.3% in II→I PT. The abrupt decrease of weight starts at about 520 K. This decomposition process is accompanied by the big exothermal peak which is characterisitic for perchlorate compounds[22,23]. During the decomposition $[Pip][ClO_4]$ looses ca 80% of its initial weight.

4 Crystal structure

4.1 Phase transitions

Piperazinium perchlorate crystalizes in the form of transparent rhombic prisms. The results of the X–ray diffraction unambiguously reveal the triclinic symmetry at room temperature. All diffraction patterns may be indexed in a unit cell: a=7.79(1)Å, b=7.96(1)Å, c=8.01(1)Å, α=104(1)°, β=108(1)°, γ=114(1)° and V=390Å^3. Detailed inspection of the collected data revealed however additional, weak peaks that indicated formation of larger "superstructure". Taking into account these patterns the unit cell at room temperature is defined by following metrics: a=7.96(1)Å, b=8.01(1)Å, c=12.66(1)Å, α = 84(1)°, β = 88(1)°, γ = 76(1)° and V=726Å^3.

Due to the crystal ability for second harmonic generation the non–centrosymmetric $P1$ space group has been chosen for the structure refinement at room temperature and 200 K although the refinement in centrosymmetric $P\bar{1}$ space group resulted in more satisfying values of the displacement parameters for almost all atoms. With temperature increase, during phase IV to phase III transition the translational symmetry of the crystal has not been altered. Also the intensity and the number of the weak "superstructure" peaks has not changed compare to

room temperature data. Taking into account vanishing of the SHG signal in phase III the refinement of the crystal structure has been performed in $P\bar{1}$ symmetry. The next structural PT at T=417 K induced monoclinic $C2/m$ symmetry. The transformation was very abrupt, associated with considerable reconstruction of the reciprocal lattice. The intensities of the selected triclinic peaks that were measured with temperature increasing have vanished at the transition point. At the same time the quality of the measured sample has worsened. The changes reflected in the lower accuracy of the unit cell determination, especially in the high standard deviation for the monoclinic beta angle. Nevertheless, the crystal structure has been successfully determined. The last PT to Phase I was related to further worsening of the quality of the sample manifesting in the fast decay of the diffracted intensities. After cooling the crystal from phase II to room temperature it transforms to the triclinic system but after cooling from Phase I to room temperature the diffraction peaks have not appeared. It indicates that above 433 K the process of decomposition of $[Pip][ClO_4]$ under the X–ray radiation is not reversible. Since DSC method showed that crystals of $[Pip][ClO_4]$ underwent the sequence of the PTs even several times for one sample the process of decomposition observed during diffraction can be activated by the X–rays and the exposition on high temperature for several hours. In summary, taking into account the SHG signal and its temperature evolution the crystal structures have been refined in the following space groups: $P1$ (Phase V), $P\bar{1}$ (Phase III), $C2/m$ (Phase II). The question which has not been solved is the symmetry and molecular configuration of the prototype Phase I. The unit cell in Phase II may also be described in nonstandard setting with body (I) centered lattice for which angle is close to 90° (a=8.348(5)Å, b=9.700(3)Å, c=10.096(9)Å and $\beta = 90.5(1)^\circ$). Therefore, the transition from Phase I to II may be associated with symmetry increase to the orthorhombic system.

4.2 The crystal structure of triclinic Phases III and V

The asymmetric unit of Phase V ($P1$ space group) consists of four independent perchlorate ions and four piperazinium counterions. After the transition to the Phase III ($P\bar{1}$ group) the number of symmetrically independent groups is reduced to two for both species. The ellipsoid representation of the asymmetric units of both phases are shown in figure S1 and S2 in supplementary materials. The ClO_4^- groups are embedded among hydrogen bonded piperazinium chains that propagate along [1 $\bar{1}$ 0] direction. Figure 2 illustrates the packing of the crystal structure as well as hydrogen bonded piperazinium chains in triclinic phases.

Despite the fact that at 200 K several oxygen atoms are in a bonding distance short enough to act as acceptors in hydrogen N—H…O bonds (table S2), significant dynamic of perchlorate that manifest in the large displacement parameters for oxygen atoms indicate that only temporary hydrogen interactions may appear. Stable N—H…N hydrogen bonds are formed between neighboring piperazinium ions with donor (D) to acceptor (A) distances ranging from 2.82(1)Å to 2.90(1)Å and D—H…A angle ranging from 157.5° to 173.3°. After the transition the hydrogen bonds elongate insignificantly and range from 2.90(1)Å to 2.92(1)Å (see table 3).

4.3 The crystal structure of Phase II

Above T=417 K, an abrupt crystal structure transformation leads to the change of the crystal system from triclinic to monoclinic with $C2/m$ space group in the first order PT. In the new Phase II perchlorate groups appear to rotate freely along the axis defined by Cl(1)—O(1) bond. Both atoms lie on the .m. mirror plane. The content of the asymmetric unit which consists in phase II of one independent perchlorate and two piperazinium counterions, along with an atom numbering scheme is presented in figure S3. The most pronounced changes are observed in the hydrogen bonded piperazinium chains. The neighboring piperazinium rings significantly change their orientation in respect to each other. The rotation angle (defined as the N(1)—N(1)'—N(2)—N(2)') torsion angle) equals ca 94°. The angle between the planes (in each piperazinium ring defined by the carbon atoms) changes from 72° to 84°. The conversion of the chains is illustrated in figure 3 whereas the packing of the crystal structure is shown in figure 4.

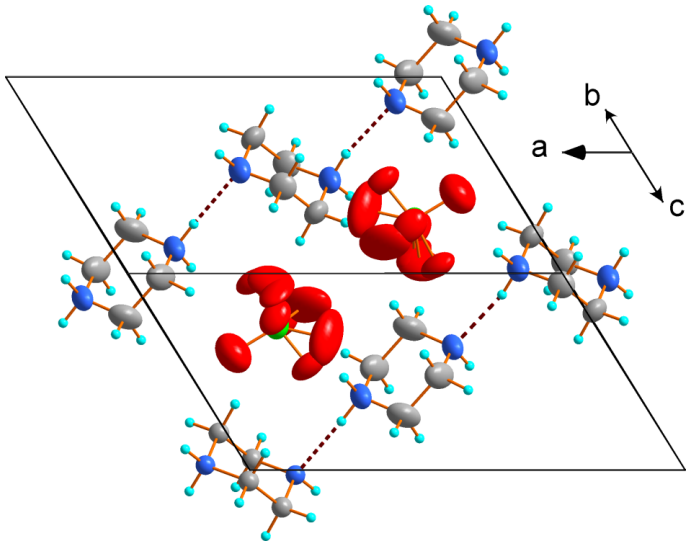

Fig. 4 The motifs of the crystal structure of the high temperature phase II, T=426 K, $C2/m$ space group. The disorder of ClO_4 groups manifests in splitting positions, statistically occupied with large displacement parameters; here drown at 30% probability.

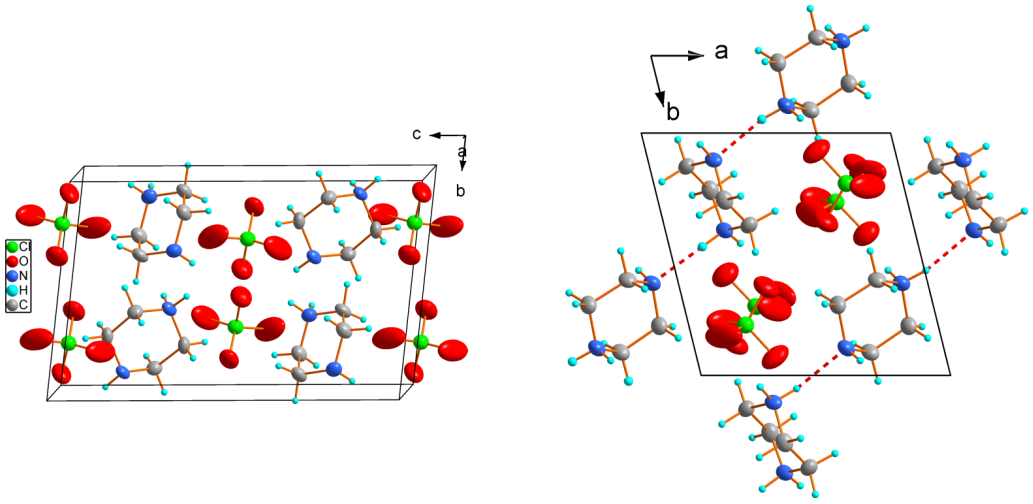

Fig. 2 Packing of the crystal structure of [Pip][ClO_4] at 413 K; the view along *c* direction with exposed chains of hydrogen bonds (dashed lines) that propagate along [1 $\bar{1}$ 0] direction. Disorder of ClO_4^- groups manifests in the huge displacement parameters of oxygen atoms which are drown at 30% probability level. For the picture clarity the splitted oxygen positions are not drown.

Table 3 Selected hydrogen–bond parameters at 200 K, 413 K and 426 K

Phase V	*T=200 K*			
D—*H*...*A*	*D*—*H* (Å)	H...A (Å)	*D*...*A* (Å)	*D*—*H*...*A* (°)
N1—H1A...N4^{i}	0.9	1.97	2.861 (7)	168.4
N4—H4C...N1^{ii}	0.9	1.98	2.856 (7)	162.9
N3—H3C...N2^{iii}	0.9	2.01	2.902 (9)	169.6
N2—H2B...N3^{iv}	0.9	2.02	2.902 (9)	166.1
N5—H5C...N8^{iv}	0.9	2.02	2.904 (6)	168.3
N8—H8C...N5^{i}	0.9	2.05	2.901 (6)	157.5
N7—H7C...N6^{iv}	0.9	1.93	2.823 (8)	173.3
N6—H6D...N7^{iii}	0.9	1.96	2.823 (8)	161.5
Symmetry code(s): (*i*) x, y+1, z; (*ii*) x-1, y, z; (*iii*) x, y-1, z-1; (*iv*) x, y-1, z.				
Phase III	*T=413 K*			
D—*H*...*A*	*D*—*H* (Å)	H...A (Å)	*D*...*A* (Å)	*D*—*H*...*A* (°)
N1—H1A...N4^{i}	0.9	2.05	2.922 (4)	163.7
N2—H2B...N3^{ii}	0.9	2.04	2.899 (4)	159.1
N3—H3C...N2^{iii}	0.9	2.01	2.899 (4)	171.5
N4—H4D...N1^{vi}	0.9	2.06	2.922 (4)	159
Symmetry code(s): (*i*) x, y-1, z; (*ii*) x-1, y, z; (*iii*) x+1, y, z; (*vi*) x, y+1, z.				
Phase II	*T=426 K*			
D—*H*...*A*	*D*—*H* (Å)	H...A (Å)	*D*...*A* (Å)	*D*—*H*...*A* (°)
N2—H3A...N1	0.9	2.00	2.899 (9)	176.9
N1—H1B...N2	0.9	2.02	2.899 (9)	165.9

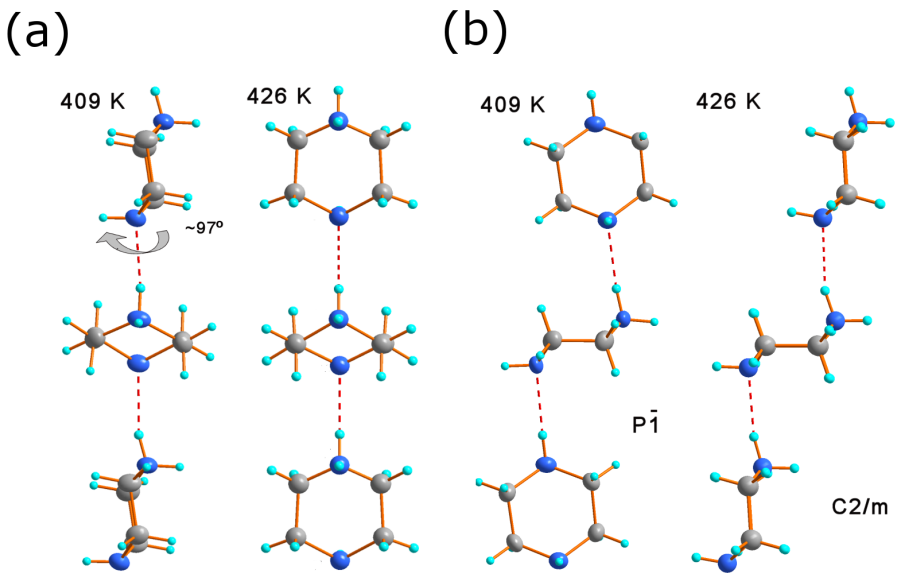

Fig. 3 Rotation of the piperazinium rings after the PT to monoclinic phase with $C2/m$ symmetry. (a)–(b) two different projections.

The oxygen positions are multiplied and statistically occupied with site occupation factor equal to 0.5 for O(21) and O(22) and 0.25 for O(31) and O(32), respectively. All the changes seem not to alter the mutual distances of piperazinium counter–ions along the hydrogen bonds which continue to show the same geometry as in the triclinic phases. The number of independent hydrogen bonds is reduced to two with D to A distance of 2.90(1)Å and D—H...A angles equal to 176.9° and 165.9°. In $C2/m$ group the geometry implies statistical distribution of hydrogen atoms as far as the nitrogen atoms in one piperazinium ring are symmetrically equivalent.

4.4 Polar properties of piperazinium perchlorate

All hydrogen bonded piperazinium chains spread in the same [1 $\bar{1}$ 0] direction in the crystal structure. The $P1$ symmetry does not restrict the direction of hydrogen bonds propagation. All the elemental dipole moments along the hydrogen bonds could be set up or down the [1 $\bar{1}$ 0] axis. However, such an arrangement would result in strong polar properties of the compound and would exclude the presence of centrosymmetric space groups in the system as far as the introduction of the inversion centre would have to conjugate with a movement of hydrogen atoms along the hydrogen bond of 2.9 Å which is unlikely. Weak SHG signal and pyroelectric responses as well as the presence of the symmetry centre at high temperatures imply the equilibrium number of chains propagating up and down in all phases. Figure 5 illustrates possible settings of the chains in subsequent phases. In phase II, with $C2/m$ symmetry there is one independent chain built of two non–equivalent piperazinium ions. Each of them, however, has the symmetry dependent nitrogen atoms which introduce disorder of hydrogen along the hydrogen bonds. The symmetry implicates the equilibrium number of up and down chains. In phase III with $P\bar{1}$ space group the symmetry of piperazinium lowers and the disorder of hydrogen atoms vanishes. However, the symmetry centre reverses the chains and the resultant dipole moment is zero. In phase V, there are two independent chains with elemental dipoles set in opposed direction. The difference in hydrogen bonds geometry between the chains may introduce an uncompensated dipole moment.

5 Pyroelectricity and Second Harmonic Generation (SHG)

The results of pyroelectric current and SHG measurements results are presented in the figure 6. The small peak of pyroelectric current at c.a. 397 K may be assigned to V→IV PT. The amperage of the current is of the order of tens of picoamperes, which is relatively small considering the area of the sample about 25 mm^2 (see e.g.[24] or[25]). In spite of the relatively large noise/signal ratio in our measurement one may observe the another anomaly of pyroelectric current plotted vs. temperature at 403 K, i.e. IV→III PT. Despite the small magnitude of the anomalies of pyroelectric current they coincide well with PTs temperatures. The number of anomalies of pyroelectric current detected on our experiment is consistent with the X-ray measurements which suggest that V↔IV↔III PTs

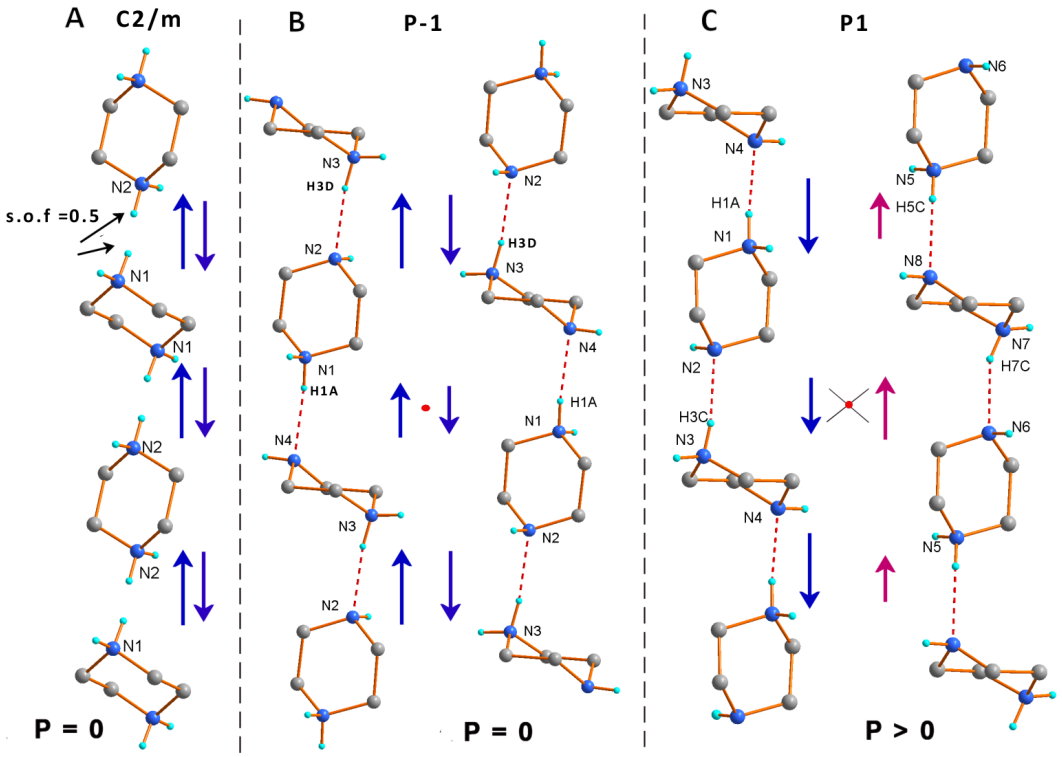

Fig. 5 The hydrogen bonded chains of [Pip][ClO_4] in phases II-V. In phase II the hydrogen atoms along the chains are statistically disordered with site occupation factor of 0.5. In all phases there is an equilibrium number of hydrogen bonds with dipoles directed up and down the chains.

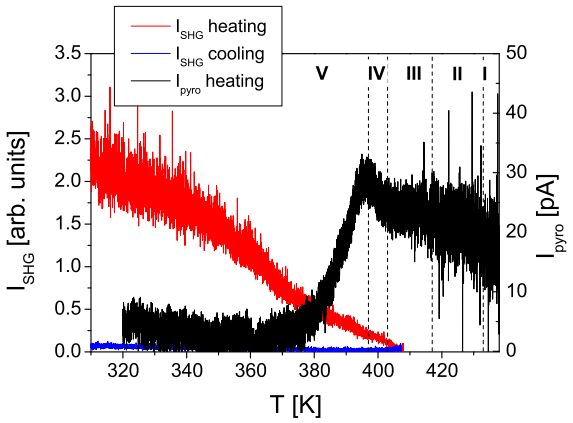

Fig. 6 Pyroelectric current along the [1 $\bar{1}$ 0] direction and SHG intensity of $[Pip][ClO_4]$.

are linked with subtle deformation of hydrogen bond system of $[Pip][ClO_4]$.

Attempts to change the spontaneous polarization direction by the external electric field (up to 1000 kV/m) were unsuccessful, which suggests that the compound under investigation may be classified as a pyroelectric one.

SHG is an optical, noncontact probe method is applicable even to powdered samples. The SHG measurements clearly proof the noncentrosymmetric character of the room temperature phase (V). When temperature of the sample incresases the intensity of the SHG signal diminishes and drops to 0 in the phase III. The SHG measurement is not fully repetitive most probably due to the partial decomposition of the sample under the laser irradiation. Namely,the signal recorded on cooling is over one order of magnitude lower than that on heating. $[Pip][ClO_4]$ seems to decompose when exposed to high energy radiation, which was observed also in the course of X–ray diffraction data collecting. Note, the SHG signal is reproducible when the laser beam is evenly distributed over the sample – the signal on heating is much more intensive than that on cooling. The shape of SHG signal indicates that the V↔IV↔III PTs are of the first order type.

The SHG efficiency of the piperazinium perchlorate was evaluated by using the Kurtz and Perry powder technique [16] with Potassium Dihydrogen Phosphate (KDP) as a reference material (see details in e.g.[26]). The peak intensity of SHG signal (at RT in the beginning of heating/cooling run) was about 0.8 of the value for KDP for powder size $> 125\mu$m, which gives effective SHG efficiency d= 0.94·d(KDP).

6 Dielectric measurements

Figure 7 presents the results of the temperature dependence of the electric response measured along the [1 $\bar{1}$ 0] direction (i.e. the direction which is the nonzero component of H–bond chain) of $[Pip][ClO_4]$ on heating and cooling. It must be noted that all the phase transitions are reflected in the dielectric response of studied crystal and the results are fully consistent with those obtained with other techniques, for example DSC and TGA methods. One may observe four anomalies on heating and three on cooling. The most interesting feature of the observed response is the abrupt jump of ε' at II→I PT point (see fig. 7) and then its the monotonic decrease in phase I. Such a shape of dielectric response is typical of antiferroelectric crystals at the antiferroelectric→paraelectric transformation[2]. This transformation is well reproducible, though the enhanced high ε" values in phase I are related to high conductivity of sample in this phase. In turn this phenomenon must be due to the partial decomposition of the sample as it was shown by means of TGA technique. It must be emphasized, however, that on cooling the dielectric response of both, ε' as well as ε", is fully repeatable. Moreover no relaxation processes were detected in any phases of $[Pip][ClO_4]$ in studied radio frequencies region.

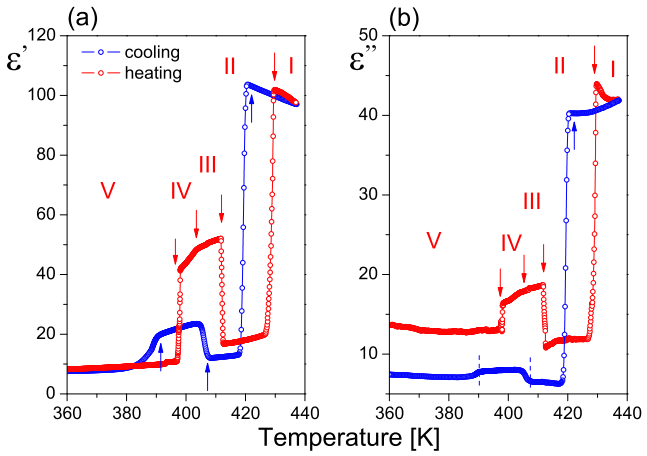

Fig. 7 The dielectric response of the $[Pip][ClO_4]$ sample measured along [1 $\bar{1}$ 0] direction at the frequency f=2 MHz recorded on heating and cooling – (a) temperature dependence of the real part of the complex electric permittivity, ε'; (b) temperature dependence of the imaginary part of the complex electric permittivity, ε"

7 NMR measurements

The temperature dependence of the experimental spin–lattice relaxation T_1 of proton ^1H (measured at 25 MHz) as a function of inverse of temperature (1000/T [K^{-1}]) is presented in Fig. 8. The spin–lattice relaxation T_1 time shows weak dependence on temperature at low temperatures with T_1 times of

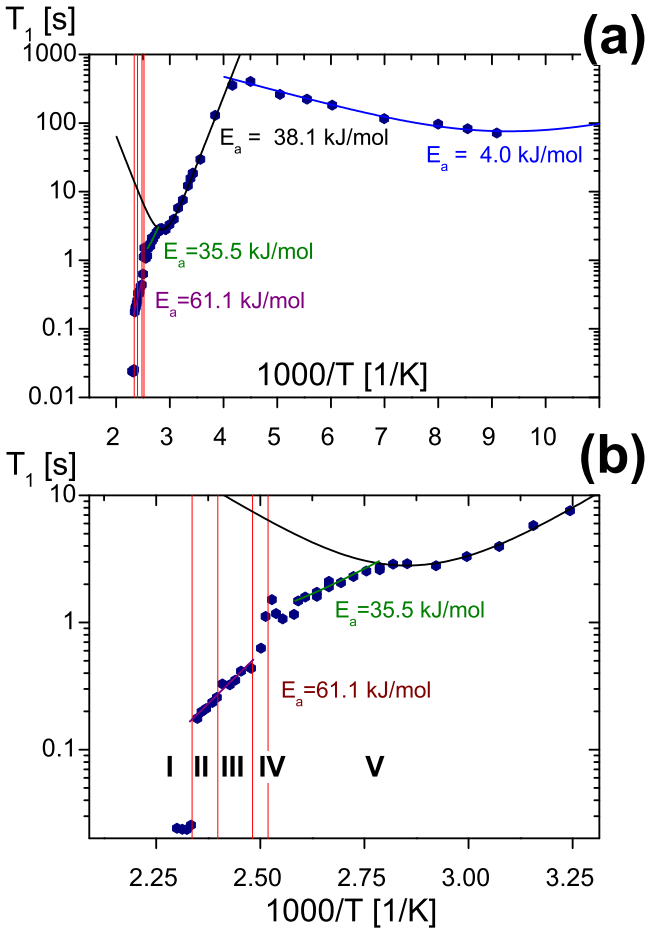

Fig. 8 The temperature dependence of the experimental spin-lattice relaxation T_1 of proton ^1H (measured at 25 MHz) as a function of inverse of temperature (1000/T [K^{-1}]) in the whole studied temperature range (a) and in the range 300–450 K (b).

the order of a hundred seconds. In the whole studied temperature range the relaxation function is one exponential and T_1 up to about 220 K is given by the BPP equation for thermally activated classical motion:

$$\frac{1}{T_1} = C_{HH}\left(\frac{\tau_c}{1+\omega_0^2\tau_c^2} + \frac{4\tau_c}{1+4\omega_0^2\tau_c^2}\right) \quad (1)$$

where relaxation constant depends on the mode of motion and correlation time τ_c is expressed by the Arrhenius relation $\tau_c = \tau_0 \exp(E_a/RT)$. A numerical fit of the experimental data (solid line in Fig. 8) yields the following parameters: $E_a = 4.1$ kJ/mol, $\tau_c = 4.2 \times 10^{-11}$ s and $C_{HH} = 1.4 \times 10^6$ s^{-2}. These parameters probably describe the motion of the one isolated proton between two positions of double–well potential located along the hydrogen bond.

Above ca. 240 K the T_1 relaxation time gradually decreases passing through four PTs at 397, 403, 417 and 433 K (on heating) – see Fig. 8b. It should be noted that the experimental points between 240 K and 351 K may be fitted with the relaxation function with the following parameters: $E_a = 38$ kJ/mol, the correlation time $\tau_c = 8 \times 10^{-12}$ s and relaxation constant 3.9×10^7 s^{-2}. The activation energies estimated numerically from data points from temperature ranges 363–386 K and 407–426 K are equal to 35.4 kJ/mol and 61.1 kJ/mol, respectively. One may note that around PTs at 397 and 403 K there are small irregularities of T_1 but above III→II PT they become negligible.

The spin–lattice relaxation time experiences a rapid drop at 433 K, i.e. the II→I PT reaching a constant value of T_1 around 24 ms. The distinctly higher E_a values found at high temperatures are probably the result of translational effects domination (like diffusion through the lattice or proton conductivity) over the reorientational motion of the piperazinium cations.

8 Discussion

The phase situation from the thermodynamic point of view (the shape of thermal anomalies and values of entropy transitions) in the crystal under investigation $[Pip][ClO_4]$ and its analog $[Pip][BF_4]$[27] reveals high similarity (see diagram below), however, the structural symmetry of corresponding phases is different.

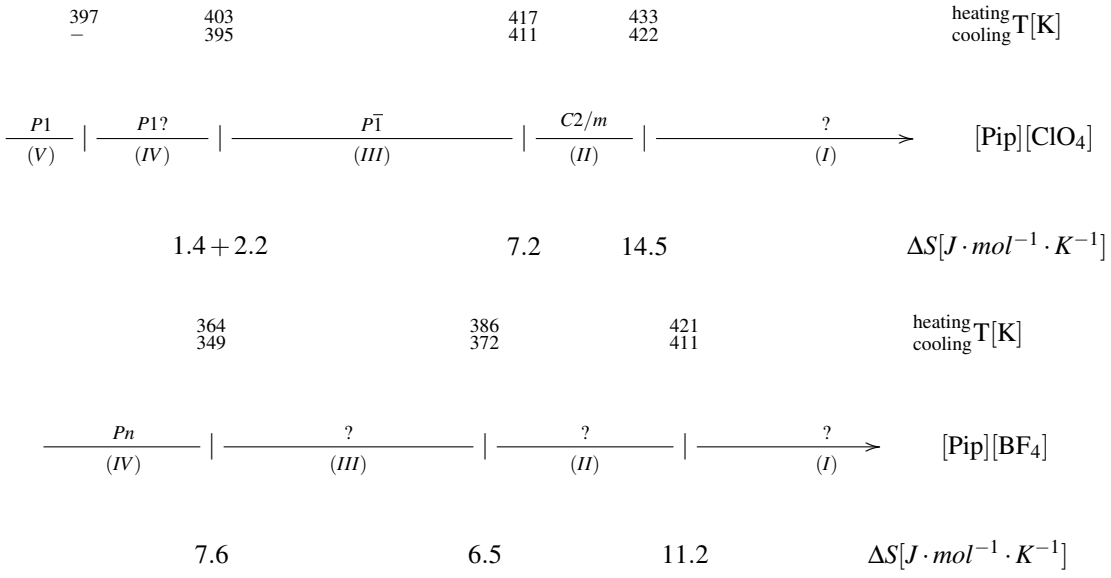

Both compounds were found to exhibit solid–solid phase transitions above room temperature. The values of the transition entropies (ΔS_{tr}) for corresponding PTs are, generally speaking, similar to each other in both salts. The highest temperature phase transitions are characterized by the largest value of ΔS_{tr} and thereby the most significant change of structure. Moreover, it should be emphasized that the total entropy effect for these two analogs are identical (about 26 $J \cdot K^{-1} \cdot mol^{-1}$), which means that the motional state of ions in the lowest and the highest temperature phases is comparable.

It is impossible to compare the microscopic mechanism of PTs in both crystals because for [Pip][BF_4] only its ordered room temperature phase IV (*Pn*) is determined. In [Pip][ClO_4] the dynamics of ClO_4^- anions play an essential role in all structural PTs, because the displacement parameters of the Cl and O atoms become larger with temperature and in the phase I we probably deal with an overall reorientation of anions. In turn, the organic chain of cations is nearly rigid up to 417 K thus they do not contribute to the V→IV and VI→III PT mechanism. Only above 417 K, in phase II, one can observe a significant change of the mutual arrangement of the neighboring piperazinium rings along the chain with the rotation angle being equal to 94° ("displacive" contribution). Since the ClO_4^- anions start to perform the free rotation along the Cl(1)—O(1) bond we deal with the "order–disorder" contribution as well.

The molecular mechanism of the PT II↔I, clearly "order–disorder" type, is postulated to be due to onset of the reorientational motion of cations related to the break of the organic chains and isotropic reorientation of the tetrahedral ClO_4^- anions. Such a mechanism is suggested by the proton magnetic resonance measurements. The PTs V→IV and II→I are well reflected in ^{1}H NMR measurements since T_1 experiences a rapid step–wise changes at these points. The lowest temperature transition is explained in terms of the change in dynamics of protons in the N—H…O hydrogen bonds, whereas the highest temperature one is due to the onset of the piperazinium cations dynamics and proton conductivity as well. The intermediate PTs IV→III and III→II are hardly visible in the ^{1}H NMR studies what confirms that the changes of ClO_4^- dynamics are those which contribute mainly to the molecular mechanism of these transitions.

The most spectacular features of the piperazinium analogs are their nonlinear optical (NLO) behavior and polar properties of room temperature phases. Both materials crystallize in the non centrosymmetric space groups (BF_4 – space group *Pn* and ClO_4 – *P*1). In the case of [Pip][ClO_4] the lack of inversion centre was confirmed by the second harmonic generation measurements whereas in the case of fluoroborate analog the piezoelectric measurements were applied. Based on the pyroelectric and X–ray measurements carried out for title crystal we can suggest that its polar character in the low temperature phase is related to the arrangement of the polar organic chains contributing to the spontaneous polarization. [Pip][ClO_4] appears to be a polar crystal over the phase V (probably also in phase IV) with quite small spontaneous polarization non reversible under an external electric field (up to 10 kV/cm) thus it may be classified as a weak pyroelectric compound. The polarity of the lowest temperature phase V in [Pip][ClO_4] resembles that of [Pip][BF_4] in phase IV.

The most significant property of [Pip][ClO_4], from the point of view of dielectric properties, is a postulated antiferroelec-

tricity over one of the intermediate phases, i.e. phase II. The characteristic increase of ε' approaching T_C(I→II) with $\varepsilon'_{max} \approx 105$ and then stepwise fall to 10 units on cooling resembles the dielectric response frequently encountered in pure antiferroelectric materials. It should be added that a similar dielectric behavior close to T_C may be observed in ferroelectric crystals, however, in such a case the lower temperature phase must be polar whereas in our case this phase (II) is centrosymmetric (non polar). Thus the dielectric characteristic close to T_C (I→II) and the significant entropy effect ($\delta S_{tr} = 14.5\ J{\cdot}K^{-1}{\cdot}mol^{-1}$) as well as a discontinuous change in the T_1 spin–lattice relaxation time of ^1H NMR confirm the freezing out of the reorientational motion of polar piperazinium cations at this PT point. It should be emphasized that antiferroelectricity is a rare phenomenon in organic materials, the CCDC crystallographic database contains only five examples of antiferroelectric crystals[28].

9 Conclusions

We synthesized new organic–inorganic hybrid crystal: $[NH_2(CH_2)_4NH][ClO_4]$. The compound was found to exhibit complex sequence of phase transitions at high temperatures (four on heating and three on cooling) which are due to the dynamics of both piperazinium and perchlorate moieties as well as a change in the disorder of protons of the N—H...N hydrogen bonds. The single protonated piperazinium cations which are involved in strong linear N—H...N hydrogen bonded chains which is an origin of the polar properties of the low temperature phases (IV and V) and possible antiferroelectricity in the phase II. It must be emphasized that the monocation in the hybrid salts of piperazinium with simple inorganic acids appears very rarely. Up to date there are merely 4 examples in CCDC database: bis(Piperazin-1-ium) tetrathiotungstate[29], Piperazinium nitrate[30], catena-(Piperazinium bis(μ2-selenido)-gallium)[31] and Piperazin-1-ium tetrafluoroborate[27]. The crystal under investigation is potentially applicable as a nonlinear optical (NLO) material because of its low cost of synthesis and good thermal stability.

Acknowledgements

This work was supported by the National Research Centre (Grant No. 2013/11/D/ST8/03297). Thanks are due to Dr. Andrzej Bil for fruitful discussion.

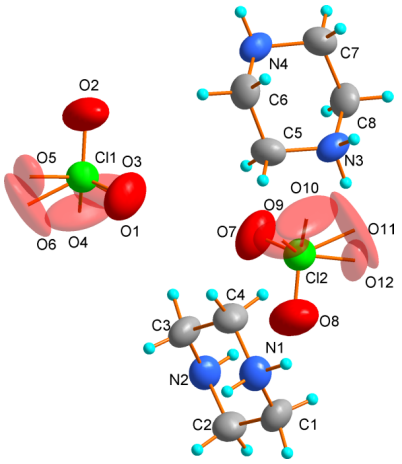

Fig. S2 Asymmetric unit of phase III, T=413 K, $P\bar{1}$ space group. Disordered atoms are made transparent. Site occupancy factor for O5, O6, O9, O10, O11 and O12 is equal to 0.5.

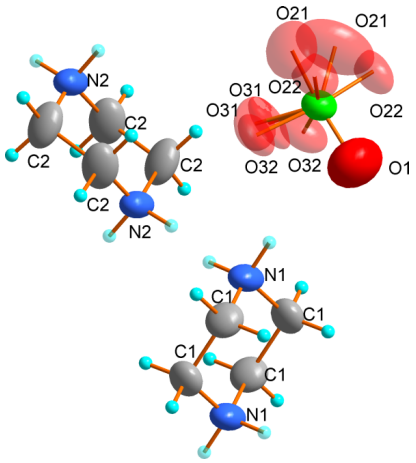

Fig. S3 Nonequivalent molecules in Phase II, the atoms from the asymmetric unit are labeled. Site occupancy factor for O22 and O21 is equal to 0.5 whereas for O31 and O32 is equal to 0.25.

10 Supplemental materials

10.1 Crystal structure

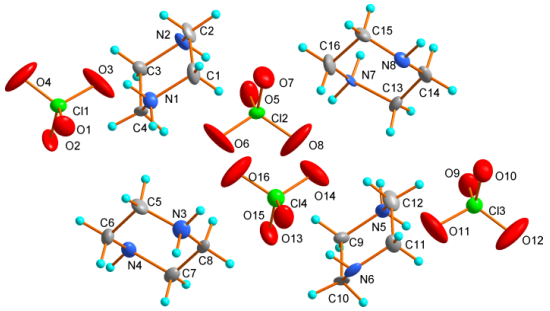

Fig. S1 Asymmetric unit in phase V, T=200 K, $P1$ space group. Disordered hydrogen atoms are made transparent.

Table S1 Selected geometric parameters (Å) at 200 K–Phase IV, (a) 426 K, at 413 K–Phase III and at 426 K–Phase II. Independent ClO_4^- groups and piperazinium counter–ions are numbered.

200 K, $P1$			
1		**2**	
Cl1—O4	1.413 (7)	Cl3—O12	1.407 (8)
Cl1—O1	1.430 (6)	Cl3—O11	1.384 (7)
Cl1—O3	1.456 (7)	Cl3—O9	1.415 (7)
Cl1—O2	1.441 (6)	Cl3—O10	1.444 (7)
3		**4**	
Cl2—O6	1.399 (7)	Cl4—O16	1.427 (7)
Cl2—O8	1.412 (7)	Cl4—O13	1.425 (6)
Cl2—O5	1.416 (6)	Cl4—O14	1.446 (7)
Cl2—O7	1.432 (7)	Cl4—O15	1.420 (7)
5		**6**	
N1—C4	1.4718 (13)	N5—C9	1.4730 (13)
N1—C1	1.4732 (13)	N5—C12	1.4718 (13)
N2—C2	1.4703 (13)	N6—C11	1.475 (9)
N2—C3	1.472 (9)	N6—C10	1.457 (6)
C1—C2	1.5004 (13)	C9—C10	1.545 (6)
C3—C4	1.504 (10)	C11—C12	1.529 (10)
7		**8**	
N3—C5	1.4718 (13)	N7—C16	1.4716 (13)
N3—C8	1.4720 (13)	N7—C13	1.4724 (13)
N4—C6	1.4704 (13)	N8—C15	1.472 (6)
N4—C7	1.4703 (13)	N8—C14	1.467 (6)
C5—C6	1.528 (6)	C13—C14	1.5003 (13)
C7—C8	1.4999 (13)	C15—C16	1.526 (6)

413 K, $P\bar{1}$			
1		**2**	
Cl1—O6	1.416 (3)	Cl2—O11	1.3989 (15)
Cl1—O4	1.397 (2)	Cl2—O10	1.397 (2)
Cl1—O3	1.398 (2)	Cl2—O7	1.4051 (17)
Cl1—O1	1.4036 (17)	Cl2—O8	1.422 (3)
Cl1—O2	1.4080 (17)	Cl2—O9	1.382 (7)
Cl1—O5	1.400 (2)	Cl2—O12	1.401 (2)
3		**4**	
N1—C1	1.464 (4)	N3—C8	1.476 (4)
N1—C4	1.470 (4)	N3—C5	1.490 (4)
N2—C3	1.428 (4)	N4—C6	1.451 (4)
N2—C2	1.440 (4)	N4—C7	1.467 (4)
C1—C2	1.514 (4)	C5—C6	1.503 (4)
C3—C4	1.515 (4)	C7—C8	1.505 (4)

426 K, $C2/m$			
1		**2**	
Cl1—O21	1.397 (2)	N1—C1	1.447 (5)
Cl1—O31	1.400 (3)	N1—C1^{i}	1.447 (5)
Cl1—O22	1.398 (2)	C1—C1^{ii}	1.484 (8)
Cl1—O1	1.401 (3)	N2—C2	1.426 (6)
Cl1—O32	1.400 (2)	N2—C2^{i}	1.426 (6)
		C2—C2^{iii}	1.498 (10)

Symmetry codes: (i) x, -y+1, z;
(ii) -x, y, -z+1; (iii) -x+1, y, -z+2

Table S2 Selected hydrogen-bond parameters at 200 K, 413 K and 426 K

200 K, P1				
D—*H*…*A*	*D*—*H* (Å)	H…A (Å)	*D*…*A* (Å)	*D*—*H*…*A* (°)
N1—H1A…N4i	0.89	1.99	2.858 (7)	165.6
N1—H1B…O2i	0.89	2.05	2.917 (9)	164.9
N2—H2A…O7	0.89	2.20	3.053 (10)	161.3
N3—H3C…N2iii	0.89	2.02	2.905 (9)	173.7
N3—H3D…O15	0.89	2.36	2.938 (9)	122.4
N3—H3D…O16	0.89	2.45	3.258 (9)	151.6
N4—H4D…O10v	0.89	2.44	3.064 (9)	127.6
N5—H5C…N8ii	0.89	2.02	2.901 (9)	170.6
N5—H5D…O10ii	0.89	2.05	2.907(9)	161.3
N6—H6C…O15	0.89	2.20	3.078 (9)	168.9
N7—H7C…N6iv	0.89	1.96	2.839 (8)	170.1
N7—H7D…O7	0.89	2.39	2.978 (8)	123.4
N7—H7D…O14	0.89	2.46	3.015 (10)	120.4
N8—H8D…O2vi	0.89	2.46	3.074 (9)	126.9
N8—H8D…O4vi	0.89	2.59	3.457 (11)	163.8

Symmetry code(s): (i) x, y+1, z; (ii) x-1, y, z; (iii) x, y-1, z-1; (iv) x, y-1, z; (v) x+1, y, z; (vi) x, y+1, z+1.

413 K, P-1				
D—*H*…*A*	*D*—*H* (Å)	H…A (Å)	*D*…*A* (Å)	*D*—*H*…*A* (°)
N1—H1A…N4i	0.9	2.05	2.922 (4)	163.7
N1—H1B…O2i	0.9	2.08	2.961 (4)	166.5
N1—H1B…O3i	0.9	2.55	3.254 (10)	135.8
N2—H2A…O8	0.9	2.26	3.145 (5)	168.9
N2—H2B…N3ii	0.9	2.04	2.899 (4)	159.1
N3—H3C…N2iii	0.9	2.01	2.899 (4)	171.5
N3—H3D…O8iv	0.9	2.31	3.005 (4)	133.6
N3—H3D…O12iv	0.9	2.33	3.135 (9)	149.3
N4—H4C…O2v	0.9	2.44	3.152 (4)	135.9
N4—H4C…O5v	0.9	2.50	3.341 (11)	154.8
N4—H4D…N1vi	0.9	2.06	2.922 (4)	159

Symmetry code(s): (i) x, y-1, z; (ii) x-1, y, z; (iii) x+1, y, z; (iv) -x+1, -y+1, -z+1; (v) -x+1, -y+2, -z+2; (vi) x, y+1, z.

426 K, C2/m				
N2—H3A…N1	0.9	2.00	2.899 (9)	176.9
N1—H1B…N2	0.9	2.02	2.899 (9)	165.9

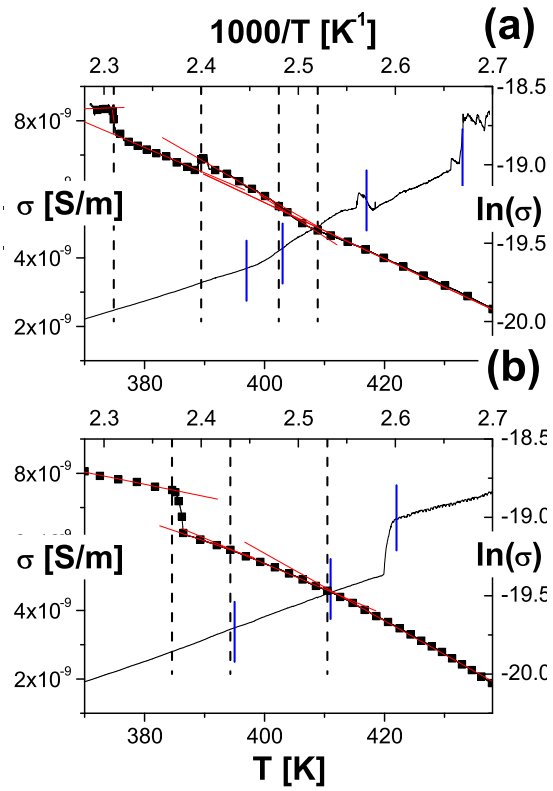

Fig. S4 Direct current conductivity vs. temperature and $\ln(\sigma_{DC})$ vs. reciprocal temperature on heating (a) and cooling (b). The thin line is the electrical conductivity, short blue lines stand for PTs. The point–line data are $\ln(\sigma_{DC})$, the long dotted lines stand for PTs in reciprocal temperature scale. The red lines are the fit of $\ln(\sigma_{DC})$.

10.2 DC conductivity measurements

The measurements of electrical conductivity were carried out on the sample along [1 $\bar{1}$ 0] direction in order to examine the possible proton conductivity in hydrogen bonds N—H...N. The results are presented in figure S4. The reciprocal temperature dependence of $\ln\sigma_{DC}$ in each phase followed the Arrhenius formula:

$$\sigma_{DC} = A_0 \cdot \exp\left(\frac{E_a}{RT}\right), \qquad (2)$$

where σ_{DC}, A_0, E_a and R stand for conductivity at direct current, preexponential factor, activation energy and the gas constant, respectively. The following table presents the obtained values of activation energy.

	E_a [kJ/mol]
phase I	10.5
phase II	17.4
phase III	21.9
phase V	29.0

All the values are in the range 10–30 kJ/mol and diminish with increasing temperature. Such a values were encountered for some ionic conductors such as 0.5 Ag_2S—0.5 Ge_2S[32], $[C(NH_2)_3]_2SbCl_5x[C(NH_2)_3]Cl$[33], α–TMAOH[34], Ag_2HfS_3[35] or $H_3Mo_{12}PO_{40} \cdot 29H_2O$ and $H_3W_{12}PO_{40} \cdot 29H_2O$[36]. However, the values of DC conductivity of the title crystal are distinctly lower than conductivity of compounds mentioned above. In spite of this the mechanism of conductivity seems to be the same, i.e. proton transfer along hydrogen bond. The rise of conductivity with temperature point at changes of dynamical state of proton in hydrogen bond. The abrupt change of DC conductivity at II↔I PT, however, may be related to additional contribution of other types of ions to conductivity process. It might be due to the high disorder in crystal structure in phase I suggested by the X–ray and DSC measurements.

References

1 J. Ravez, *Chemistry*, 2000, **3**, 267.
2 G. A. Smolenskij, B. Hilczer, C. Pawlaczyk and N. N. Krajnik, *Ferroelektryki i antyferroelektryki*, Państwowe Wydaw. Naukowe, 1971.
3 C. Kittel, *Introduction to Solid State Physics*, John Wiley & Sons, Inc., New York, 6th edn, 1986.
4 G. Xu, G.-G. Guo, M.-S. Wang, Z.-J. Zhang, W.-T. Chen and J.-S. Huang, *Angew. Chem. Int. Ed.*, 2007, **46**, 3249.
5 Q. Ye, D.-W. Fu, H. Tian, R.-G. Xiong, P. W. H. Chan and S. D. Huang, *Inorg. Chem.*, 2008, **47**, 772.
6 D.-W. Fu, W. Zhang and R.-G. Xiong, *Cryst. Growth Des.*, 2008, **8**, 3461.
7 P. Czarnecki, W. Nawrocik, Z. Pająk and J. Wąsicki, *J. Phys.: Condens. Matter*, 1994, **6**, 4955.
8 P. Czarnecki, W. Nawrocik, Z. Pająk and J. Wąsicki, *Phys. Rev. B*, 1994, **49**, 1511.
9 J. Wąsicki, P. Czarnecki, Z. Pająk, W. Nawrocik and W. Szczepański, *J. Chem. Phys.*, 1997, **107**, 576.
10 Z. Pająk, P. Czarnecki, J. Wąsicki and W. Nawrocik, *J. Chem. Phys.*, 1998, **109**, 6420.
11 Z. Pająk, H. Małuszyńska, B. Szafrańska and P. Czarnecki, *J. Chem. Phys.*, 2002, **117**, 5303.
12 A. Katrusiak and M. Szafrański, *Phys. Rev. Lett.*, 1999, **82**, 576.
13 M. Szafrański, A. Katrusiak and G. J. McIntyre, *Phys. Rev. Lett.*, 2002, **89**, 215507–1.
14 H.-L. Cai, D.-W. Fu, Y. Zhang, W. Zhang and R.-G. Xiong., *Phys Rev. Lett.*, 2012, **109**, 169601.
15 I. Nishiyama, *Adv. Mater.*, 1994, **6**, 966.
16 S. K. Kurtz and T. T. Perry, *J. Appl. Phys.*, 1968, **39**, 3798.
17 Oxford Diffraction, *CrysAlis system software, CrysAlis CCD and CrysAlis RED*, 2001.
18 G. M. Sheldrick, *Acta Cryst. 2008, A*, 2008, **64**, 112–122.
19 A.L.Spek, *Acta Cryst.*, 2009, **D65**, 148.
20 H. D. Flack, *Acta Cryst.*, 1983, **A39**, 876.
21 R. W. W. Hooft, L. H. Straver and A. L. Spek, *J. Appl. Cryst.*, 2008, **41**, 96.
22 R. J. Acheson and P. W. M. Jacobs, *J. Phys. Chem.*, 1970, **74**, 281.
23 M. M. Markowitz, D. A. Boryta and J. H. Stewart, *J. Phys. Chem.*, 1964, **68**, 2282.
24 M. Wojtaś, J. Zaleski, W. Medycki and R. Jakubas, *J. Phys.: Condens. Matter*, 2007, **19**, 236221.
25 M. Wojtaś, R. Jakubas, Z. Ciunik and W. Medycki, *J. Solid State Chem.*, 2004, **177**, 1575.
26 M. Wojtaś, O. Czupiński, Z. Tylczyński, D. Isakov, M. Belsley and R. Jakubas, *Chem. Phys.*, 2014, **441**, 59.
27 M. Wojtaś, A. Gągor, O. Czupiński, W. Medycki and R. Jakubas, *J. Solid State Chem.*, 2012, **187**, 35.
28 I. R. Thomas, I. J. Bruno, J. C. Cole, C. F. Macrae, E. Pidcock and P. A. Wood, *J. Appl. Cryst.*, 2010, **43**, 362.
29 B.R.Srinivasan, A.R.Naik, M.Poisot, C.Nather and W.Bensch, *Polyhedron*, 2009, **28**, 1379.
30 G.J.Perpetuo and J.Janczak, *Acta Crystallogr.,Sect.E:Struct.Rep.Online*, 2005, **61**, o2531.
31 X. Bu, N. Zheng, X. Wang, B. Wang and P. Feng;, *Angew.Chem.,Int.Ed.*, 2004, **43**, 1502.
32 B. Durand, G. Tallades, A. Pradel, M. Ribes, J. C. Badot and N. Belhadjtahar, *J . Non-Cryst. Solids*, 1994, **172**, 1306.
33 J. Zaleski, G. Bator and R. Jakubas, *Z. Naturforsch.*, 1995, **50(a)**, 888.
34 M. Opallo, A. Tymosiak and Z. Borkowska, *J. Electroanal. Chem.*, 1995, **387(1-2)**, 47.
35 H. Wada, O. Amiel and A. Sato, *J. Alloys Compounds, 219, 55.*, 1995, **219**, 55.
36 O. Nakamura, T. Kodama, I. Ogino and Y. Miyake, *Chem. Lett.*, 1979, **8**, 17.

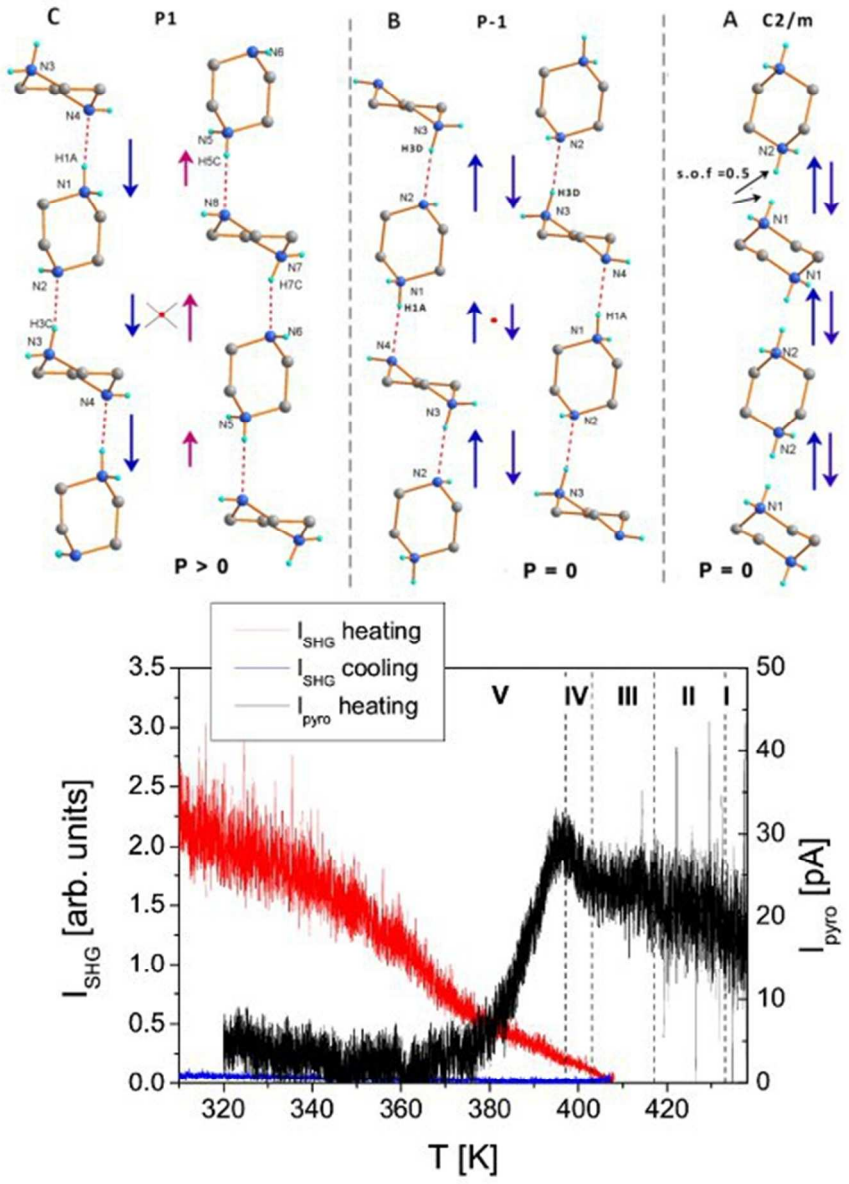

The hydrogen bonded chains of [Pip][ClO4] in phases II-V and vs. SHG and pyroelectric current response.
47x60mm (300 x 300 DPI)